scientific reports

Check for updates

OPEN

Green synthesis of hematite nano flakes and their application as a counter electrode in dye-sensitized solar cells

Emma Panzi Mukhokosi[1,2]✉, Emmanuel Mushebo[1], Stella Nassejje[2], Nandipha L. Botha[3], Dhayalan Velauthapillai[4] & Malik Maaza[3]

This study pioneers using hematite nanoflakes as a viable alternative to traditional platinum counter-electrodes in dye-sensitized solar cells (DSSCs), demonstrating its effectiveness for the first time. Besides such a novelty, the used hematite nanoflakes were bio-engineered using ginger extract as an effective chelating reducing agent. From the X-ray diffraction studies, it was observed that the sample annealed at 700 °C formed a highly crystalline α-Fe_2O_3, with a crystallite nano-scaled size of the order of 46.3 nm. The scanning electron microscopy investigations indicated a preferred layered nanoflakes morphology while the optical properties revealed a direct band gap of 2.30 eV. Using N-719 dye as a sensitizer on TiO_2 photoanode and I^-/I_3^- as electrolyte, the DSSC was fabricated. Such a cell exhibited significant DSSC responses, namely; a short circuit current density (J_{SC}) of 7.0 mAcm^{-2}, an open circuit voltage (V_{OC}) of 389 mV, and a fill factor (FF) of 75.3% in addition to an efficiency (η) of 2.05%. Based on such a significant photo-conversion response using bio-engineered active counter electrodes, this study provides a cost-effective approach for synthesizing hematite NFs that have potential applications not only in DSSC but also in sensors, water splitting, and electrochemical devices.

Keywords Hematite nano flakes, Green synthesis, Ginger' natural extract, Photo-conversion, DSSC

For decades, researchers have focused on 2D nanosystems, particularly nano-flakes of layered nanomaterials, which offer high specific surface areas, active sites, and unique surface properties. These characteristics make them ideal for various applications, including solar cells, where they enhance electron transport kinetics, ion diffusion, and charge transfer[1–5].

The growing global demand for renewable energy has intensified the need for efficient and affordable solar energy solutions. Dye-sensitized solar cells (DSSCs) have emerged as a promising alternative to traditional silicon solar cells, offering ease of fabrication, acceptable efficiency, and mechanical flexibility[6–8]. The concept of DSSCs originated in 1887, with the photosensitization of organic dyes, and was later modified by Michael Grätzel[9]. A typical DSSC consists of a dye-sensitized photoanode, an electrolyte, and a counter electrode as seen schematically in Fig. 1[10] (Copyright © 2014 John Wiley & Sons, Ltd).

The counter electrode plays a major role in reducing I_3^- to I^- in the electrolyte[11]. The catalytic properties of counter electrodes in DSSCs depend on the surface area, alignment of crystal planes, and the porosity of the particles[12]. Traditionally, platinum (Pt) is used as the counter electrode in DSSCs, owing to its exceptional electron mobility, low internal resistance, and outstanding catalytic properties[11]. Nevertheless, platinum's rarity, high cost, and tendency to dissolve in the electrolyte, forming toxic complexes, pose significant drawbacks[13]. These limitations render DSSCs expensive, unstable, and environmentally hazardous, hindering their widespread adoption and commercial viability. Consequently, there is a pressing need to develop alternative, platinum-free counter electrodes for DSSCs[14].

Hematite (α-Fe_2O_3), is an abundant mineral with excellent catalytic activity and hence a potential substitute for Pt[8,15]. The key attractive properties of hematite nanostructures are; large surface areas, good conductivity, and a narrow band gap (1.90–2.50 eV) enabling them to be adopted in several applications such as DSSCs, water

[1]Department of Physics, School of Natural and Applied Sciences, Kampala International University, P.O Box 20000, Kampala, Uganda. [2]Department of Physics, Faculty of Science, Kyambogo University, P.O Box 1, Kyambogo, Uganda. [3]UNESCO UNISA Africa Chair in Nanosciences & Nanotechnology, College of Graduate Studies, University of South Africa, Pretoria, South Africa. [4]Faculty of Engineering and Science, Western Norway University of Applied Sciences, 5063 Bergen, Norway. ✉email: epmukhokosi@kyu.ac.ug; panzi2018@gmail.com

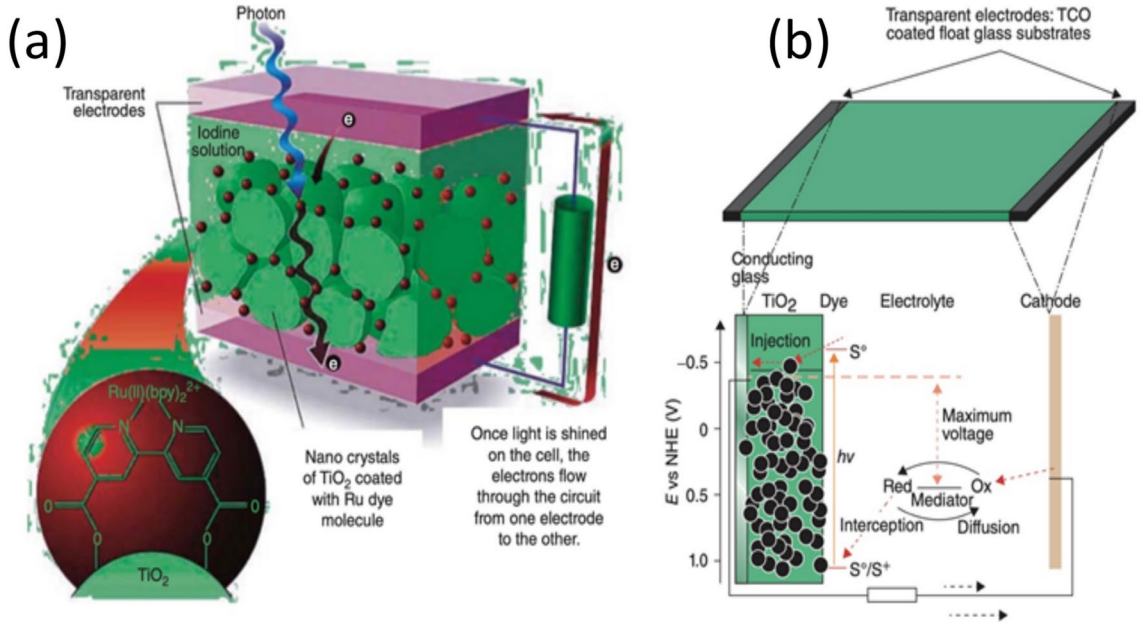

Fig. 1. (**a**) Principle of electron generation in a Grätzel DSC via excitation of dye molecules (small spheres) coating nano-TiO_2 mesoporous film, (**b**) Schematic representation of the various physical–chemical reactions taking place in a standard DSC unit. Figures (**a**) and (**b**) were reproduced with permission from reference[10].

splitting, photodetectors, and photocatalysis[16–20]. The hematite nanostructures have been synthesized by Physical and chemical methods[21–23]; however, the Physical methods are expensive and occasionally involve the use of large quantities of chemicals hence not sustainable[24]. Hematite nanoparticles (NPs) have been prepared by a variety of chemical methods such as Sol–Gel, chemical precipitation, hydrothermal/solvothermal, co-precipitation, template-assisted methods, solvent thermal method, electrochemical synthesis, and green synthesis[25,26]. Among these methods, green synthesis has gained attention due to its simplicity and cheapness. Green synthesis utilizes bio-active compounds in plant extracts, microorganisms, and any other sustainable sources to develop NPs[27]. Among the plant extracts, ginger contains gingerols and terpenoids with hydroxyl (–OH) and carbonyl (–C=O) functional groups[27,28]. These functional groups are capable of reducing $Fe_2Cl_3.6H_2O$ into Fe^{3+}, Fe^{2+}, and Fe^0 leading to the growth of nanoparticles of different morphologies of iron oxide.[21] The crystallinity, particle size, optical, and surface morphology of the nanostructures in green synthesis technique highly depends on the pH, reaction time, and reaction temperature. This study investigates the bio-engineering of hematite nanoflakes using ginger extract and their possible use as an effective counter electrode in DSSCs. To determine if they could be utilized as a platinum substitute in DSSC applications, an evaluation of their structural, optical, morphological, and photovoltaic response is considered. As validated further down, the optical properties revealed a direct energy band gap of 2.30 eV. Using N-719 dye as a sensitizer and I^-/I_3^- as an electrolyte, the DSSC based on the nano-scaled hematite flakes as a counter electrode revealed J_{SC} of 7.0 $mAcm^{-2}$, V_{OC} of 389 mV, and FF of 75.3% with an efficiency, η of 2.05%. Based on such a preliminary set of results, and besides the validation of the effectiveness of a bio-engineered hematite counter-electrode based DSSC, this contribution seems pointing to the possibility of application in sensors, water splitting, and electrochemical devices, among others.

Materials and methods

Materials

Ginger rhizomes were sourced from a local market in Bulambuli District, Eastern Uganda. The vendors were informed about the intended use of the ginger rhizomes for scientific research, and their consent was obtained prior to procurement, Ferric chloride anhydrous (98% purity), ethanol (96%), distilled water, TiO_2 powder (particle size < 25 nm (anatase phase) were purchased from Sigma Aldrich), N-917 dye 95% (NMR) purchased from Zhengzhou Alfa chemical Ltd, Potassium iodide ($\geq$ 99.0%), Iodine ($\geq$ 99.8%, solid), Acetonitrile ($\geq$ 99.9%), Ethylene glycol (99.8%), glacial acetic acid (100%), The fluorine-doped tin oxide (FTO) coated glass substrates (6.7 ± 0.27 Ω/square cm, obtained from Ossila Ltd-UK).

Preparation of ginger extract

Figure 2 summarizes the flow chart for experimental procedures followed for the bio-engineering of the hematite NFs using ginger rhizome extract. The Ginger rhizomes were washed thoroughly using tap water, followed by distilled water. They were then dried in an oven, and finally ground using a standard mortar and pestle to obtain a fine powder. 20 g of such a ginger powder was added to 0.2 L of DI and boiled at 70 °C on a magnetic hotplate with continuous stirring for 30 min. The mixture was then filtered via a Whatman filter paper (Cat No 1440-

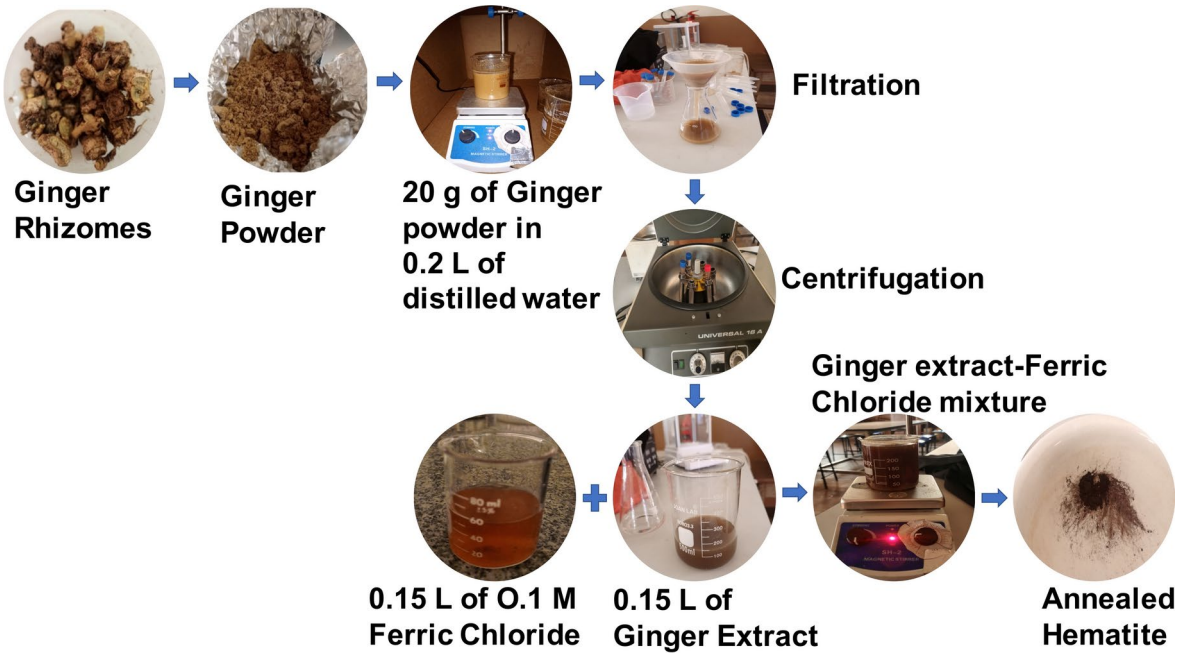

Fig. 2. Flow chart for experimental procedures demonstrating the use of ginger extract in the green production of iron oxide.

125) of pore size 8 µm and centrifuged (UNIVERSAL 16A) at room temperature for 10 min at 2400 rotations per minute (rpm).

Synthesis of α-Fe_2O_3 nanoparticles

3.24 g of $FeCl_3.6H_2O$ was added into 0.1 L of distilled water and then topped with an adequate amount of distilled water to make 0.2 L, resulting in a 0.1 M solution. 0.15 L of ginger extract was mixed with 0.15 L of $FeCl_3.6H_2O$ in a conical flask. The mixture was stirred at 70 °C for 120 min. As a result, a dark brown precipitate was produced. The precipitate was then placed in an oven at 120 °C for 12 h. Thereafter, the powder was collected in a boat and calcinated in a muffle furnace at various temperatures, namely; 400 °C, 500 °C, 600 °C, and 700 °C for 2 h.

Preparation of DSSC photoanode

The FTO-coated glass substrates were submerged in a beaker with an equal mixture of deionized water and ethanol, and then subjected to ultrasonic cleaning for 15 min. The substrates were gently removed and left to dry in a dust-free environment. The FTO substrates were side-covered with a one layer of scotch tape, which had a thickness of 0.06 mm. The photoanode paste was prepared by mixing 1 g of TiO_2 powder, 6 mL of glacial acetic acid, 6 mL of DI water, and 300 mg of polyethylene glycol, and the mixture was sonicated for three hours. 0.2 ml of the paste was drop cast on FTO glass substrate and allowed to dry in a clean environment. The thin film was annealed at 400 °C in a muffle furnace for thirty minutes[29]. The furnace was cooled to room temperature naturally. The TiO_2-coated on FTO substrate was soaked in a 0.5 mM ruthenium (II) 535 bis-TBA (N-719) dye solution for 24 h at room temperature in a dark environment[30,31]. The substrate was removed, rinsed with methanol, and dried to obtain a dye-sensitized photoanode. The photoanode was kept in a homemade dark box for further use.

Preparation of the DSSC counter electrode

A mixture containing 0.5 g of pure phase hematite NFs, 8 mL of ethanol, and 0.12 g of polyethylene glycol was ultrasonicated for 3 hours[15]. The paste was drop-cast on the FTO substrate and annealed in a muffle furnace at 400 °C for 30 minutes[29]. The thickness of the α-Fe_2O_3 thin film was estimated to be 0.06 mm.

Preparation of the electrolyte

A mixture containing 830 mg of potassium iodide (KI) powder, 10 mL of ethylene glycol, and 27 mg of I_2 crystals was stirred for 30 min in a dark environment and a dark-brown solution was obtained[32,33]. The mixture was stored in amber bottles for further investigation.

Materials characterization

The crystal structural properties were investigated using an X-ray diffractometer (SHIMADZU XRD 7000 with CuKα irradiation at λ = 1.5406 Å). The surface morphology and elemental composition were investigated using Scanning electron microscopy (FESEM, Jeol JSM-7400F)[31]. The optical properties were investigated using a UV–visible–NIR spectrophotometer[34].

DSSC assembling and *J–V* measurements

The dye-sensitized TiO_2 photoanode and the α-Fe_2O_3 counter electrode were assembled firmly using clips with an active area of 0.15 cm^2. A micro syringe was used to inject the electrolyte into the DSSC through the micro space left between the photoanode and the counter electrode. The device was illuminated with 1 sun (100 mW/mW^{-2}) and the J–V characteristics were recorded using Keithley 2450-SMU.

Results and discussion

Phase composition and structural properties

Figure 3a shows the XRD pattern of the synthesized samples at different annealing temperatures. The diffraction data were compared with the data files in the Joint Committee on Powder Diffraction Standards (JCPDS card no. 33-0664) database. The XRD pattern show that the material had impurity phases for calcination temperatures below 400 °C. With increasing calcination temperatures, the impure phases transformed into a pure phase at 700 °C. The peaks were indexed to (012), (104), (110), (006), (113), (024), (116), (018), (214), (300), (1010), and (220) planes corresponding to 2θ = 24.2°, 33.2°, 35.7°, 39.4°, 40.9°, 49.5°, 54.1°, 57.7°, 62.5°, 64.1°, 72.0°, and 75.5° respectively. These planes correspond to a rhombohedral structure with an R $\bar{3}$ c space group. The crystallite size was calculated using Debye Scherrer's approximation (1).

$$D = \frac{\lambda k}{\beta_{hkl}\cos\theta_{hkl}} \tag{1}$$

where D is the size of the crystallite, λ is the X-ray radiation wavelength, θ_{hkl} is the Bragg's angle, $k = 0.9$ is the shape factor, and β_{hkl} is the full width at half-maximum (FWHM) intensity. The major peak was identified and the hematite NFs that were annealed at 400 °C, 500 °C, 600 °C, and 700 °C had average crystallite sizes of 20.9 nm, 27.2 nm, 35.0 nm, and 46.3 nm, respectively, demonstrating that crystallite size increases with annealing temperature. The lattice parameters of the pure phase sample at 700 °C were estimated from two peaks (104) and (110) with maximum intensity using (2).

$$\frac{1}{d^2} = \frac{4}{3}\left(\frac{h^2 + hk + k^2}{a^2}\right) + \frac{l^2}{c^2} \tag{2}$$

where h, k, and l are miller indices of the crystal lattice with a = 5.0124 Å, b = 5.0124 Å, and c = 13.7620 Å, which are close to those reported in the literature[35].

The atom configuration in the haematite unit cell is illustrated in Fig. 3b. The iron ions (Fe^{3+}) are surrounded by six oxygen ions (O^{2-}) in octahedral positions. These octahedral forms form a three-dimensional network via sharing edges. Oxygen ions occupy the vertices of the octahedral and coordinate with the three Fe^{3+} ions. If one considers the labels "p, q, r, s, t, u" as corresponding to the oxygen atoms in the polyhedral coordination surrounding a core Fe^{3+} ion (identified as "A"). Accordingly, the bond length between the oxygen ions is 2.9421 Å for p-r, p-q, and q-r, 2.8542 Å for p-t, r-u, and q-s, 2.8076 Å for t-u, s-u, and s-t, and 2.7999 Å for q-u, s-p, and r-t. These comparatively large distances suggest the existence of mutually repelling forces between similarly charged oxygen ions. Atoms A-u, A-s, and A-t have an iron-oxygen bond length of 2.1328 Å, while atoms A-q, A-p, and A-r have a length of 1.9234 Å. Compared to the other three, this indicates that three of these oxygen atoms are marginally closer to the iron atom. Therefore, when electrons are present in an oxygen ion's outermost shells, it results in a slightly distorted octahedron.

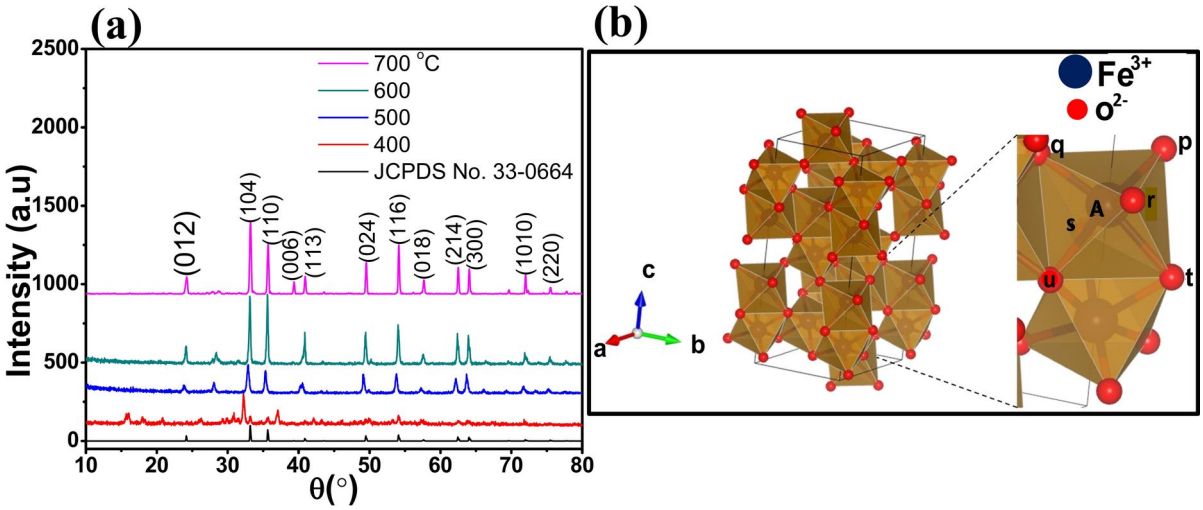

Fig. 3. (**a**) XRD pattern of synthesized hematite nanoflakes. (**b**) Crystal lattice structure illustrating the unit cell of synthesized hematite nanoflakes.

Surface morphology and chemical composition

Figure 4a and b respectively show the SEM micrograph and EDX spectrum of the hematite NFs annealed at 700 °C, revealing the formation of highly agglomerated platelet nano-flakes with excellent crystallinity. Rajendran et al. have shown that the (110) plane indicates hematite NFs are oriented in the [110] direction[36]. From the XRD results, the (110) plane was not observed at a calcination temperature of 400 °C but observed at 500, 600, and 700 °C, suggesting that the hematite NFs are oriented in the [110] direction. The SEM micrographs in Fig. 4c and d confirm this observation, revealing the presence of NFs. In contrast, no NFs were detected in the as-synthesized sample (Fig. 4e). Notably, the crystallinity and orientation of the bio-engineered hematite NFs exhibited a positive correlation with calcination temperature, increasing as the temperature rose. The atomic weight percentage of 34.84% for O and 65.16% for Fe were obtained and were in proper stoichiometry for hematite.

Optical properties

Figure 5a shows the diffuse reflection spectra (DRS) of hematite NFs. The DRS was converted to equivalent absorbance spectra using the Kubelka–Munk function shown in Fig. 5b. The absorbance was determined from the Eq. (3).

$$F(R) = \frac{(1-R)^2}{2R} \tag{3}$$

where *F(R)* is the Kubelka–Munk function and *R* is the reflectance factor at the surface of the sample. The band gap was estimated as shown in Fig. 5c using Tauc plots obtained using Eq. 4. A band gap of 2.30 eV was estimated[37].

In Eq. 4, $F(R) = \alpha$

$$(\alpha h\upsilon)^{\gamma} = A(h\upsilon - E_g) \tag{4}$$

Figure 5d shows the absorbance spectrum for the prepared N-719 Ruthenium dye. Two prominent peaks at 383 nm and 525 nm were observed and is in accordance with other reports[38].

J–V characteristics

The hematite nano-flakes calcined at 700 °C were crystalline and hence used to fabricate a counter electrode. The counter electrode plays the role of reduction of the I_3^- to I^- in the DSSC as illustrated by Eq. (5).

$$I_3^- + 2e^- \rightarrow I^- \tag{5}$$

The detailed internal processes involving electron transfer mechanisms are reported in the literature[39]. The power conversion efficiency η was computed using (6)[40].

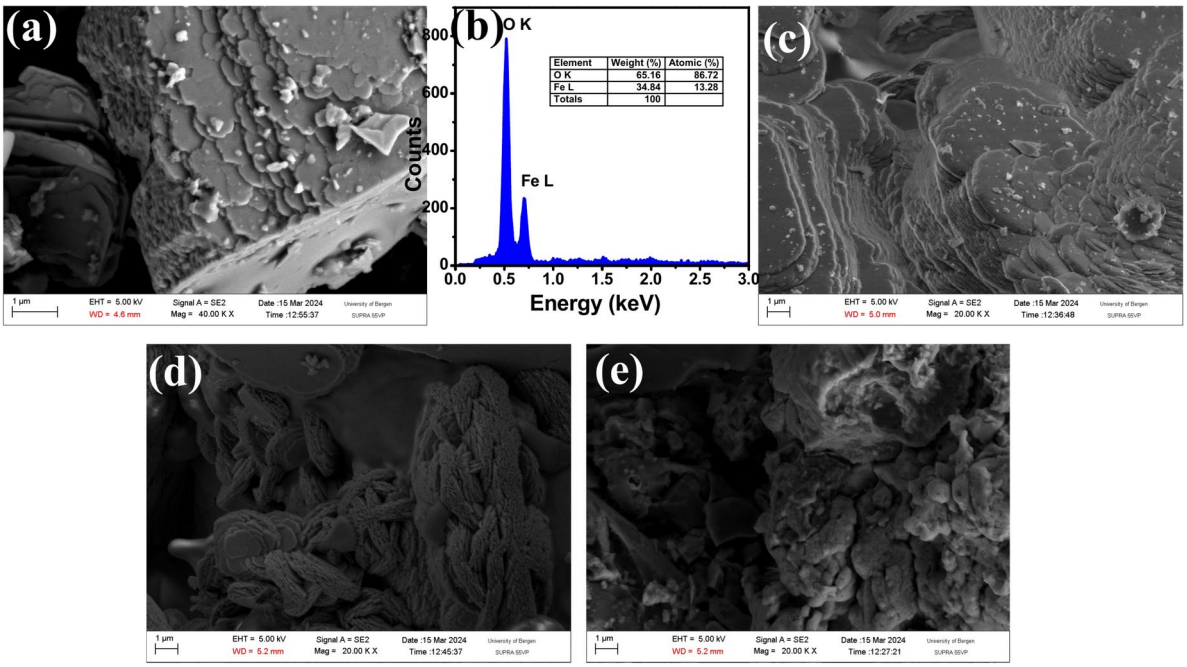

Fig. 4. SEM micrographs of synthesized iron oxide NFs calcined at; (**a**) 700 °C with its EDX spectrum (**b**), (**c**) 600 °C, (**d**) 500 °C, and (**e**) as-synthesized sample.

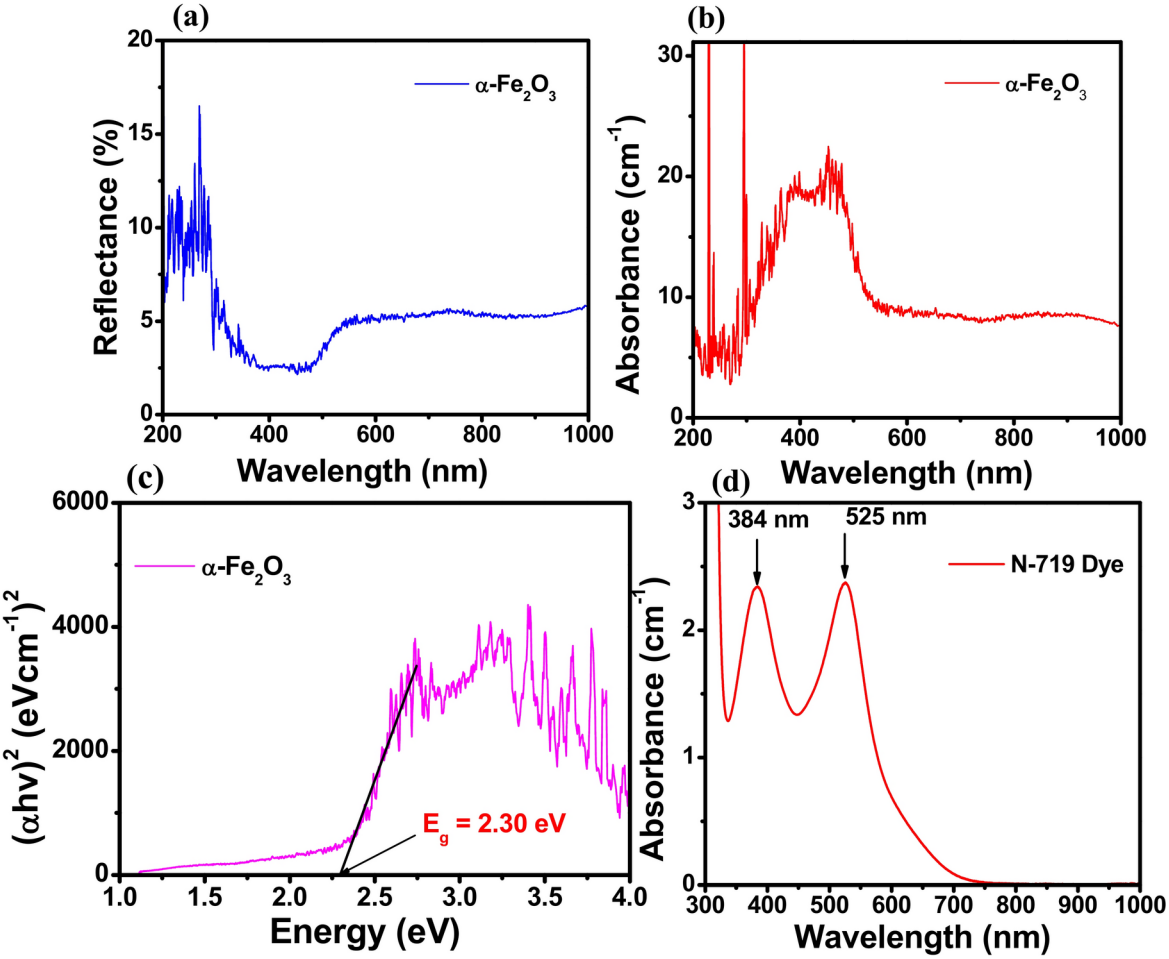

Fig. 5. (**a**) DRS of α-Fe_2O_3 nano flakes calcined at 700 °C, (**b**) Absorbance spectrum of α-Fe_2O_3 nano flakes, (**c**) Tauc plot of α-Fe_2O_3 nano flakes calcined at 700 °C, and (**d**) Absorbance spectrum of the N-719 dye.

$$\eta = \frac{J_{cs}\left(\mathrm{mAcm^{-2}}\right) \times V_{oc}\,(\mathrm{V}) \times \ \mathrm{FF}}{P_{in}(mWcm^{-2})} \tag{6}$$

and

$$\mathrm{FF} = \frac{\mathrm{P_{max}(mWcm^{-2})}}{J_{cs} \times V_{oc}(\mathrm{mWcm^{-2}})} \tag{7}$$

Figure 6a shows the *J–V* characteristics of the DSSC fabricated DSSC device under 1 sun illumination. Figure 6b shows the variation of power density of the cell with voltage.

The cell based on bioengineered α-Fe_2O_3 nano flakes as a counter electrode revealed a J_{SC} of 7.0 $mAcm^{-2}$, V_{OC} as 389 mV, and *FF* of 75.30% giving η as 2.05%. These *J–V* parameters are comparable with previous reports[15]. An open circuit photo-voltage of 389 mV was largely attributed to the strong interaction between the semiconductors and the electrolyte due to the size and large surface area of the hematite nano-flakes. The low values of P_{max} and η can be attributed to higher recombination rates in the redox coupler (KI/I_2).

Conclusions

In summary, a cost-effective, non-toxic, and eco-friendly approach was used to synthesize α-Fe_2O_3 nano-flakes. The findings revealed the formation of highly crystalline α-Fe_2O_3 nano flakes with a crystallite size of 46.3 nm and a plate-like morphology having a band gap of 2.30 eV. The developed solar cell based on the α-Fe_2O_3 nano-flakes as a counter electrode revealed a power conversion efficiency of 2.05%. Although this strategy for synthesizing α-Fe_2O_3 NFs using ginger extract as a reducing/stabilizing agent was successful, the power conversion efficiency of the solar cell was much lower as compared to the conventional Platinum counter electrode[31]. Further studies on thickness control and other alternative thin film deposition techniques such as dip-coating can improve the efficiency of the DSSC cell using α-Fe_2O_3 NFs as a counter electrode. In addition, other plant materials can be investigated to synthesize α-Fe_2O_3 nanoparticles of different dimensions. Further

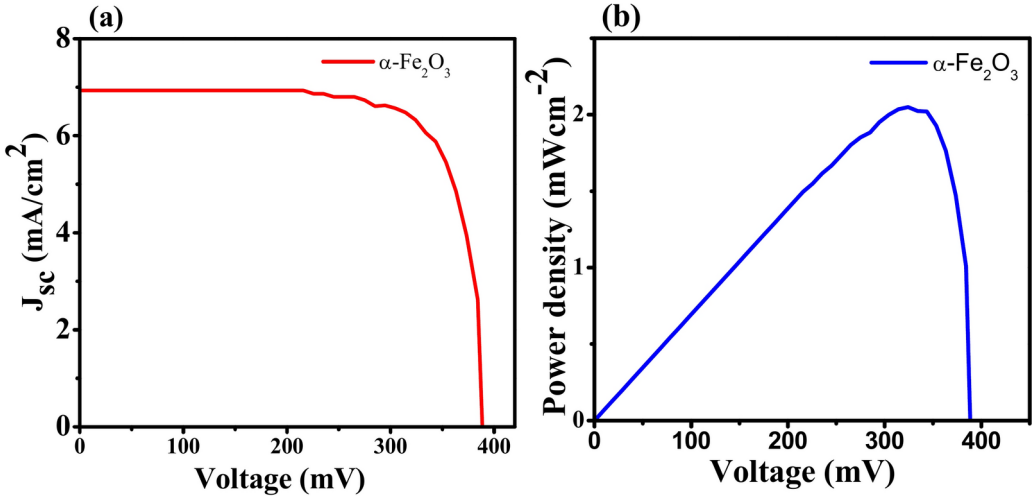

Fig. 6. (**a**) *J*–*V* graph of fabricated DSSC using hematite as a counter electrode, and (**b**) variation of the power density of the DSSC with Voltage.

studies on the use of a Lithium Iodide (LiI) as an electrolyte, determination of oxidation states of α-Fe_2O_3 NFs using X-ray photoelectron spectroscopy, charge transfer resistance/dynamics, and band alignments at the interface can enhance understanding of the synthesized material and fabricated device.

Data availability

The datasets used and/or analyzed during the current study are available from the corresponding author on reasonable request.

Received: 17 October 2024; Accepted: 18 March 2025
Published online: 05 June 2025

References

1. Naz, I. et al. Green synthesis of NiO nanoflakes using bitter gourd peel, and their electrochemical urea sensing application. *Micromachines* https://doi.org/10.3390/mi14030677 (2023).
2. Wang, W., Wu, Y., Wu, Q., Hua, J. & Zhao, J. Coherent nonlinear optical response spatial self-phase modulation in $MoSe_2$ nanosheets. *Sci. Rep.* **6**, 1–6 (2016).
3. Fabbri, F. et al. Novel near-infrared emission from crystal defects in MoS_2 multilayer flakes. *Nat. Commun.* **7**, 1–7 (2016).
4. Huang, X., Pan, K. & Hu, Z. Experimental demonstration of printed graphene nano-flakes enabled flexible and conformable wideband radar absorbers. *Sci. Rep.* **6**, 4–11 (2016).
5. Pozina, G., Forsberg, M., Kaliteevski, M. A. & Hemmingsson, C. Emission properties of Ga_2O_3 nano-flakes: Effect of excitation density. *Sci. Rep.* **7**, 1–8 (2017).
6. Deb, S. K. Dye-sensitized TiO_2 thin-film solar cell research at the national renewable energy laboratory (NREL). *Sol. Energy Mater. Sol. Cells* **88**, 1–10 (2005).
7. Devadiga, D., Selvakumar, M., Shetty, P. & Santosh, M. S. Dye-sensitized solar cell for indoor applications: A mini-review. *J. Electron. Mater.* **50**, 3187–3206 (2021).
8. Ahmed, U. et al. A comprehensive review on counter electrodes for dye sensitized solar cells: A special focus on Pt-TCO free counter electrodes. *Sol. Energy* **174**, 1097–1125 (2018).
9. Kay, A. & Grätzel, M. Artificial photosynthesis. 1. Photosensitization of TiO_2 solar cells with chlorophyll derivatives and related natural porphyrins. *J. Phys. Chem.* **97**, 6272–6277 (1993).
10. Maaza, M. *Natural Dyes for Photonics Applications* Vol. 6, 479–493 (Wiley, 2014).
11. Pang, E. C. L. & Chow, W. K. A low-cost, high-efficiency solar cell based on dye-sensitized colloidal TiO_2 films. *Nature* **353**, 737–739 (1991).
12. Jasim, K. E. Dye Sensitized Solar Cells - Working Principles, Challenges and Opportunities. *B. Chapter* (2007).
13. Mariotti, N. et al. Recent advances in eco-friendly and cost-effective materials towards sustainable dye-sensitized solar cells. *Green Chem.* **22**, 7168–7218 (2020).
14. Olsen, E., Hagen, G. & Eric Lindquist, S. Dissolution of platinum in methoxy propionitrile containing LiI/I2. *Sol. Energy Mater. Sol. Cells* **63**, 267–273 (2000).
15. Shahpari, M., Behjat, A., Khajaminian, M. & Torabi, N. The influence of morphology of hematite (α-Fe_2O_3) counter electrodes on the efficiency of dye-sensitized solar cells. *Sol. Energy* **119**, 45–53 (2015).
16. Ahmmad, B. et al. Green synthesis of mesoporous hematite (α-Fe_2O_3) nanoparticles and their photocatalytic activity. *Adv. Powder Technol.* **24**, 160–167 (2013).
17. Asoufi, H. M., Al-Antary, T. M. & Awwad, A. M. Green route for synthesis hematite (α-Fe_2O_3) nanoparticles: Toxicity effect on the green peach aphid, Myzus persicae (Sulzer).. *Environ. Nanotechnol. Monit. Manag.* **9**, 107–111 (2018).
18. Priya-Naveen-Kaur, K. & Sidhu, A. K. Green synthesis: An eco-friendly route for the synthesis of iron oxide nanoparticles. *Front. Nanotechnol.* https://doi.org/10.3389/fnano.2021.655062 (2021).
19. Soltys, L., Olkhovyy, O., Tatarchuk, T. & Naushad, M. Green synthesis of metal and metal oxide nanoparticles: Principles of green chemistry and raw materials. *Magnetochemistry* **7**, 11–14 (2021).
20. Kiwumulo, H. F. et al. Green synthesis and characterization of iron-oxide nanoparticles using Moringa oleifera: A potential protocol for use in low and middle income countries. *BMC Res. Notes* **15**, 1–8 (2022).

21. Steier, L. et al. Understanding the role of underlayers and overlayers in thin film hematite photoanodes. *Adv. Funct. Mater.* **24**, 7681–7688 (2014).
22. Glasscock, J. A., Barnes, P. R. F., Plumb, I. C., Bendavid, A. & Martin, P. J. Structural, optical and electrical properties of undoped polycrystalline hematite thin films produced using filtered arc deposition. *Thin Solid Films* **516**, 1716–1724 (2008).
23. Kment, S. et al. On the improvement of PEC activity of hematite thin films deposited by high-power pulsed magnetron sputtering method. *Appl. Catal. B Environ.* **165**, 344–350 (2015).
24. Oberdick, S. D. et al. Iron oxide nanoparticles as positive T1 contrast agents for low-field magnetic resonance imaging at 64 mT. *Sci. Rep.* **13**, 1–13 (2023).
25. Hou, Y. et al. Rational screening low-cost counter electrodes for dye-sensitized solar cells. *Nat. Commun.* https://doi.org/10.1038/ncomms2547 (2013).
26. Md Ishak, N. A. I., Kamarudin, S. K. & Timmiati, S. N. Green synthesis of metal and metal oxide nanoparticles via plant extracts: An overview. *Mater. Res. Expr.* **6**(11), 112004 (2019).
27. Devi, H. S., Boda, M. A., Shah, M. A., Parveen, S. & Wani, A. H. Green synthesis of iron oxide nanoparticles using Platanus orientalis leaf extract for antifungal activity. *Green Process. Synth.* **8**, 38–45 (2019).
28. More, R. D. & Janrao, D. M. Synthesis of Cuo nanoparticles by green approach using zingiber officinale (Ginger) and study of its antimicrobial applications. pp. 3229–3232 (2021).
29. Mukhokosi, E. P. et al. Optical absorption and photoluminescence properties of Cucurbita maxima dye adsorption on TiO_2 nanoparticles. *Mater. Res. Express* **10**(4), 046203 (2023).
30. Shashanka, R., Esgin, H., Yilmaz, V. M. & Caglar, Y. Fabrication and characterization of green synthesized ZnO nanoparticle based dye-sensitized solar cells. *J. Sci. Adv. Mater. Devices* **5**, 185–191 (2020).
31. Mukhokosi, E. P. et al. Co-sensitization effect of chlorophyll and anthocyanin on optical absorption properties and power conversion efficiency of dye-sensitized solar cells. *J. Korean Phys. Soc.* **84**, 858–869 (2024).
32. Alkuam, E. An effective of dye molecules with cadmium sulfide nanorods in dye sensitized solar cell (DSSCs). *Adv. Mater. Phys. Chem.* **09**, 37–47 (2019).
33. Zulkifili, A. N. B., Kento, T., Daiki, M. & Fujiki, A. The basic research on the dye-sensitized solar cells (DSSC). *J. Clean Energy Technol.* **3**, 382–387 (2015).
34. Panzi, E. et al. Green synthesis of CuO nanoparticles from Cucurbita maxima leaf extract; a platinum free counter electrode for dye sensitized solar cells. *J. Niger. Soc. Phys. Sci.* **7**, 2309 (2025).
35. Fardood, S. T. et al. Eco-friendly synthesis and characterization of α-Fe_2O_3 nanoparticles and study of their photocatalytic activity for degradation of Congo red dye. *Nanochem. Res.* **4**, 140–147 (2019).
36. Rajendran, R., Yaakob, Z., Pudukudy, M., Rahaman, M. S. A. & Sopian, K. Photoelectrochemical water splitting performance of vertically aligned hematite nanoflakes deposited on FTO by a hydrothermal method. *J. Alloys Compd.* **608**, 207–212 (2014).
37. Džimbeg-Malčić, V., Barbarić-Mikočević, Ž & Itrić, K. Kubelka-Munk theory in describing optical properties of paper (I). *Teh. Vjesn.* **18**, 117–124 (2011).
38. Wen, P., Han, Y. & Zhao, W. Influence of TiO_2 nanocrystals fabricating dye-sensitized solar cell on the absorption spectra of N719 sensitizer. *Int. J. Photoenergy* **2012**, 1–8 (2012).
39. Nazeeruddin, M. K., Baranoff, E. & Grätzel, M. Dye-sensitized solar cells: A brief overview. *Sol. Energy* **85**, 1172–1178 (2011).
40. Ooyama, Y. & Harima, Y. Photophysical and electrochemical properties, and molecular structures of organic dyes for dye-sensitized solar cells. *ChemPhysChem* **13**, 4032–4080 (2012).

Author contributions

EPM conceptualized the idea, validated the results, and reviewed the manuscript. EM prepared the samples, prepared the device, analyzed the data, and wrote the first draft of the manuscript. SN analyzed the data and revised the manuscript, NLB analyzed the data and reviewed the manuscript, MM and DV reviewed the manuscript and validated the results. The final manuscript was read and approved by all authors.

Declarations

Competing interests

The authors declare no competing interests.

Additional information

Correspondence and requests for materials should be addressed to E.P.M.

Reprints and permissions information is available at www.nature.com/reprints.

Publisher's note Springer Nature remains neutral with regard to jurisdictional claims in published maps and institutional affiliations.